ELSEVIER

Structural Safety 20 (1998) 37–49

STRUCTURAL SAFETY

Multiple design points in first and second-order reliability

Armen Der Kiureghian[a]*, Taleen Dakessian[b]

[a]*Department of Civil and Environmental Engineering, University of California, Berkeley, Berkeley, CA 94720, USA*
[b]*Space Systems Division, Boeing North American, Downey, CA 90241, USA*

Abstract

A method is developed to successively find the multiple design points of a component reliability problem, when they exist on the limit-state surface. FORM or SORM approximations at each design point followed by a series system reliability analysis is shown to lead to improved estimates of the failure probability. Three example applications show the generality and robustness of the method. © 1998 Elsevier Science Ltd. All rights reserved

Keywords: Design points; first-order reliability method; optimization algorithms; probability of failure; second-order reliability method; structural reliability; tuned-mass damper

1. Introduction

In the first-order reliability method, FORM, an approximation to the probability of failure is obtained by linearizing the limit-state surface (the boundary of the failure domain) at the "design point". This is the point on the limit-state surface that is nearest to the origin in a standard normal space obtained by a suitable transformation of the random variables. Due to the rotational symmetry and exponential decay of the probability density in the standard normal space, the design point has the highest likelihood among all points in the failure domain. It follows that the neighborhood of this point makes the dominant contribution to the failure probability integral. This property is the basis for the FORM, which in effect constructs an approximation to the failure probability integral by using the tangent plane at the design point as the integration boundary. The second-order reliability method, SORM, improves on this approximation by using a quadratic surface fitted at the design point as the integration boundary. Experience has shown that FORM and SORM approximations are sufficiently accurate for engineering purposes, provided that the design point is accurately found and no other minimum-distance points (local design points) exist on the limit-state surface [1,2].

* Corresponding author.

PII: S0167-4730(97)00026-X

The design point, denoted $\mathbf{u}^*$, is the solution to the constrained optimization problem

$$\min\{\| \mathbf{u} \| \mid G(\mathbf{u}) = 0\}, \tag{1}$$

where $\mathbf{u}$ denotes the vector of standard normal variables obtained by transforming the original random variables, and $G(\mathbf{u})$ is the limit-state function defining the reliability problem in the transformed space such that $G(\mathbf{u}) \leq 0$ denotes the failure event. To solve Eq. (1) using a gradient-based approach, starting from an initial point $\mathbf{u}_0$, a sequence of points $\mathbf{u}_i$, $i = 1, 2, \ldots$, is generated according to the rule

$$\mathbf{u}_{i+1} = \mathbf{u}_i + \lambda_i \mathbf{d}_i, \tag{2}$$

where $\mathbf{d}_i$ is a search direction vector and λ_i is a step size. Algorithms differ in their choice of $\mathbf{d}_i$ and λ_i. For example, the iHL-RF algorithm developed by Zhang and Der Kiureghian [3] and used later in this study employs

$$\mathbf{d}_i = \frac{1}{\| \nabla G(\mathbf{u}_i) \|^2} [\mathbf{u}^T \nabla G(\mathbf{u}) - G(\mathbf{u}_i)] \nabla G(\mathbf{u}_i) - \mathbf{u}_i, \tag{3}$$

where $\nabla G(\mathbf{u})$ is the gradient of the limit-state function. The step size λ_i is selected such that the inequality $\mathbf{m}(\mathbf{u}_i + \lambda_i \mathbf{d}_i) < \mathbf{m}(\mathbf{u}_i)$ holds, where $\mathbf{m}(\mathbf{u})$ is the merit function

$$\mathbf{m}(\mathbf{u}) = \frac{1}{2} \| \mathbf{u} \|^2 + c|G(\mathbf{u})|, \tag{4}$$

in which c is a parameter satisfying the condition $c > \|\mathbf{u}\| / \|\nabla G(\mathbf{u})\|$ at each step. This algorithm is globally convergent, i.e., the sequence is guaranteed to converge to a minimum-distance point on the limit-state surface, provided $G(\mathbf{u})$ is continuous and differentiable. However, as with any non-convex optimization problem, it is not guaranteed that the solution point will be the global minimum-distance point.

We define the multiple solutions of Eq. (1) as $\mathbf{u}_i^*$, $i = 1, 2, \ldots$. Associated with each solution, we define the distance $\beta_i = \| \mathbf{u}_i^* \|$, which is the corresponding "reliability index". These distances provide relative measures of importance of the design points: the smaller β_i is, the more important $\mathbf{u}_i^*$ is. The design point closest to the origin, having the smallest β_i value, is denoted the *global design point*. The remaining points, having larger distances from the origin, are denoted *local design points*.

The existence of multiple design points may cause the following problems in FORM and SORM:

1. The optimization algorithm may converge to a local design point. In that case, the FORM and SORM solutions will miss the region of dominant contribution to the failure probability integral and, hence, the corresponding approximations will be in gross error.
2. Even if the global design point is found, there could be significant contributions to the failure probability integral from the neighborhoods of the local design points. Approximating the limit-state surface only at the global design point will not account for these contributions.

At the present time, no reliable and efficient method is available to find the local solutions of Eq. (1), or to ascertain that a solution found is the global design point. One method often suggested is to repeat the analysis with different starting points and hope that all the solution points will be found. Unfortunately, it is possible for all trials to converge to the same point even when other solution points exist. Global optimization methods [4] are usually heuristic in nature and depend on the structure of the problem. To our knowledge, no previous attempts have been made to use global optimization techniques to solve the structural reliability problem defined by Eq. (1).

In this paper, a simple heuristic method is developed to find the multiple design points of a reliability problem, when they exist. Once these points are found, FORM or SORM approximations are constructed at these points and the probability of interest is computed by series system reliability analysis as the probability of the union of the approximated events (see the "multi-point" FORM and SORM methods described by Ditlevsen and Madsen [2]). The basic idea of the method is presented in the following two sections. This is followed with three examples. The first two are simple two-variable examples, which are used to graphically demonstrate the methodology. The third example is a 10-story building with a tuned mass damper, whose properties are uncertain. This problem involves 33 random variables and represents an example of practical interest.

2. Basic idea of the method

In optimization theory, a common trick to find multiple solutions to a problem is to construct "barriers" around previously found solutions, thereby forcing the algorithm to seek a new solution [5]. In the present case, since the objective function is the distance $\|\mathbf{u}\|$ from the origin, a "barrier" around a first solution point $\mathbf{u}_1^*$ [see Fig. 1(a)] can be constructed by moving the limit-state surface in the neighborhood of $\mathbf{u}_1^*$ away from the origin. We accomplish this by adding a "bulge" to the limit-state surface in the manner illustrated in Fig. 1(b). The limit-state function for the deformed surface is

$$G_1(\mathbf{u}) = G(\mathbf{u}) + B_1(\mathbf{u}), \tag{5}$$

where $B_1(\mathbf{u})$ defines the bulge fitted at $\mathbf{u}_1^*$. The specifics of the bulge are defined in the following section. Solving the optimization problem with the limit-state function $G_1(\mathbf{u})$ leads to a second solution point $\mathbf{u}_2^*$, as illustrated in Fig. 1(b). A bulge $B_2(\mathbf{u})$ is now added at $\mathbf{u}_2^*$ [Fig. 1(c)], resulting in the limit-state function $G_2(\mathbf{u}) = G_1(\mathbf{u}) + B_2(\mathbf{u})$, which can be used to seek a third solution point $\mathbf{u}_3^*$. This process is continued until all design points are found. Thus, the limit-state function for finding the m-th design point is

$$G_{m-1}(\mathbf{u}) = G_{m-2}(\mathbf{u}) + B_{m-1}(\mathbf{u}) = G(\mathbf{u}) + \sum_{i=1}^{m-1} B_i(\mathbf{u}) \tag{6}$$

As is evident in Fig. 1(b)–(c), each bulge introduces spurious minimum-distance points located at the feet of the bulge, e.g., point $\mathbf{u}_3^*$ in Fig. 1(c). Theoretically speaking, it is possible for the optimization algorithm to converge to these spurious design points. However, in practice, this does

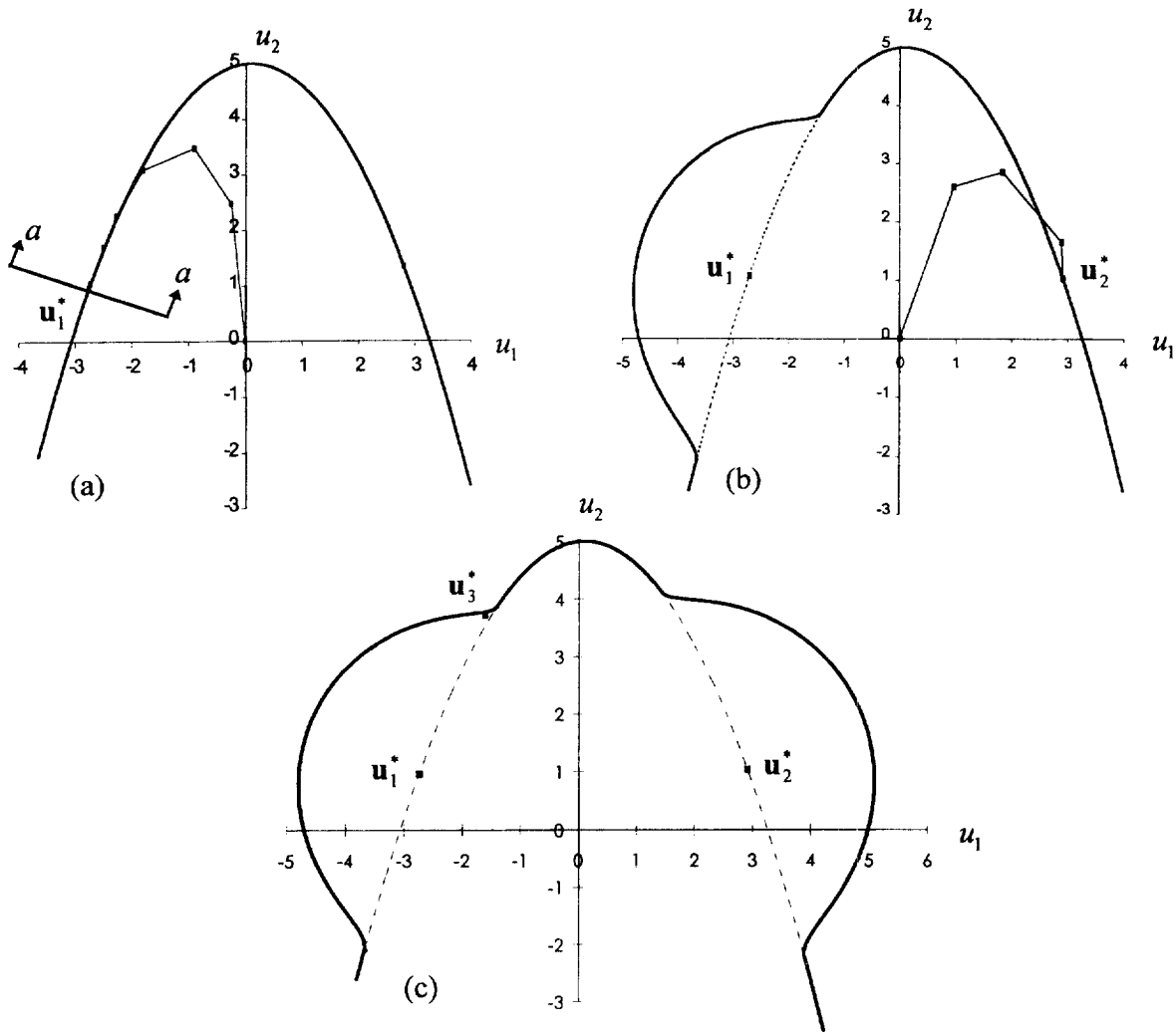

Figure 1. Successive use of bulges to find multiple design points.

not pose a problem because of the following reasons: (a) assuming the limit-state surface is not oscillatory in nature (a basic assumption for application of FORM and SORM), when multiple design points exist the surface tends to have inward curvature (curved towards the origin) at these points. On the other hand, the foot of the bulge has strong outward curvature (curved away from the origin). The iHL-RF algorithm as well as most gradient-based algorithms tend to converge more easily to solution points with inward curvature than those with outward curvature. Hence, if a genuine design point exists, it is unlikely that convergence to the foot of the bulge rather than the genuine design point will occur; (b) in the unlikely case when convergence to a spurious design point does occur, it can be easily identified in the manner described in the following section. One may then add a bulge at the spurious solution point and continue the search for genuine design

points. Our experience shows, however, that this occurs only when there is no other genuine design point. Hence, convergence to a spurious design point usually is an indication that no other genuine design point exists.

In defining the bulge in the following section, we make sure that the foot of the bulge has a strong outward curvature. Furthermore, the starting point for subsequent iterations is selected in the direction away from the previous bulges to reduce the possibility of convergence at their feet.

3. Definition of the bulge

The following considerations lead to the definition of a bulge $B_i(\mathbf{u})$ at a design point $\mathbf{u}_i^*$:

1. $B_i(\mathbf{u})$ must have a positive value in the neighborhood of $\mathbf{u}_i^*$ (in order to move the limit-state surface in this neighborhood away from the origin) and zero elsewhere.
2. For reasons described above, it is desirable that the bulge have a strong outward curvature at its feet.
3. Each of the deformed limit-state functions $G_m(\mathbf{u}) = G(\mathbf{u}) + \sum_{i=1}^{m} B_i(\mathbf{u})$ must be continuous and differentiable. Provided the original limit-state function $G(\mathbf{u})$ is continuous and differentiable, this requirement is satisfied if each $B_i(\mathbf{u})$ is continuous and differentiable. Based on this and the preceding considerations, we select

$$\begin{aligned} B_i(\mathbf{u}) &= s_i(r_i^2 - \| \mathbf{u} - \mathbf{u}_i^* \|^2)^2 \quad \| \mathbf{u} - \mathbf{u}_i^* \| \le r_i, \\ &= 0 \qquad\qquad\qquad\quad \text{elsewhere} \end{aligned} \tag{7}$$

in which r_i is the radius of the bulge and s_i is a positive scale factor. The profile of the bulge is shown in Fig. 2. Note that the second derivative of $B_i(\mathbf{u})$ at the foot $\| \mathbf{u} - \mathbf{u}_i^* \| = r_i$ is $8s_i r_i^2$. It follows that s_i and r_i must be large in order to have a strong curvature at the foot of the bulge.
4. We make the following considerations in selecting the radius r_i of the bulge: Assuming the limit-state surface is not oscillatory in nature, the multiple design points on the surface, if they exist, are usually far apart. If they are closely spaced, then owing to the smoothness of

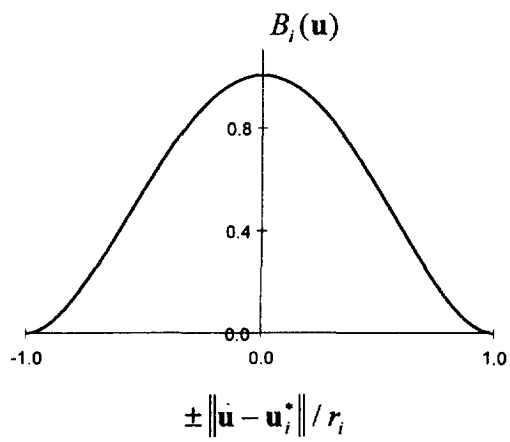

Figure 2. Profile of the bulge for $s_i = 1$.

the surface, the corresponding tangent planes must be nearly coincident, which implies that only one of these points need be considered. It follows that the radius r_i can be selected quite large without the bulge concealing other significant design points. We select $r_i = \gamma\beta_i$, where γ is a parameter. A small γ is conservative but may produce insufficient curvature at the foot of the bulge, whereas a large γ may result in a bulge that conceals other significant design points. Our experience has shown that a value of γ around 1, but not equal to 1, is a good choice. The problem with selecting $\gamma = 1$ is that the edge of the bulge coincides with the origin and this causes problems when the origin is selected as the starting point $\mathbf{u}_0$ in the optimization algorithm. In the following analyses $\gamma = 1.1$ is used.

5. The scale parameter s_i controls the height of the bulge and, hence, the distance by which the limit-state surface around $\mathbf{u}_i^*$ is moved away from the origin. s_i must be sufficiently large to assure a strong curvature at the foot of the bulge. To select this parameter, we consider the cross section a–a of Fig. 1(a), shown in Fig. 3, which is a plot of the surface $G-G(\mathbf{u})=0$ through the design point. The gradient vector normal to this surface is $[1 - \nabla G(\mathbf{u}_i^*)^T]^T$. It follows that the slope of the curve at $\mathbf{u}_i^*$ is $\tan\theta = \| \nabla G(\mathbf{u}_i^*) \|$. Suppose we want to push the design point $\mathbf{u}_i^*$ away from the origin by the amount $\delta\beta_i$, where $0 < \delta < \gamma$. It is clear from Fig. 3 that the necessary height of the bulge at that point is approximately $\delta\beta_i \tan\theta = \delta\beta_i \| \nabla G(\mathbf{u}_i^*) \|$. Using Eq. (7), this gives

$$s_i = \frac{\delta\beta_i \| \nabla G(\mathbf{u}_i^*) \|}{[(\gamma\beta_i)^2 - (\delta\beta_i)^2]^2}. \tag{8}$$

For the analyses in this paper $\delta = 0.75$ is used.

Eqs. (7) and (8) together with the parameters γ and δ completely define the bulge at each design point $\mathbf{u}_i^*$ in terms of the quantities β_i and $\| \nabla G(\mathbf{u}_i^*) \|$, which are readily available from the optimization algorithm at its convergence. Of course this definition of the bulge is not unique. For example, one can consider powers other than 2 in Eq. (7), or use an elliptical shape bulge. The bulge defined above, however, has been found through many numerical examples to be effective in tricking the optimization algorithm to converge to subsequent design points.

A further choice that needs to be made is that of the initial point $\mathbf{u}_0$. Our experience shows that this point should not be selected on the boundary of a bulge. If such a point is selected, the

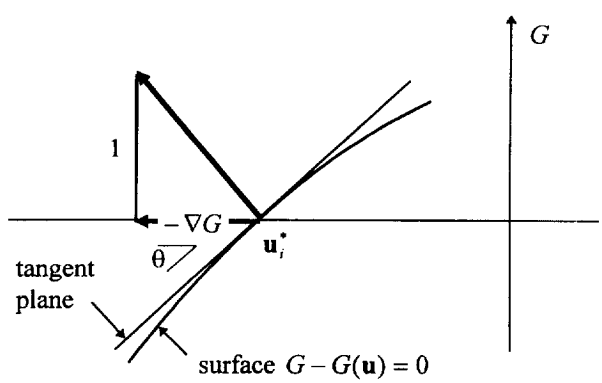

Figure 3. Cross section a–a.

optimization algorithm tends to follow the perimeter of the bulge and converge to a spurious design point at the foot of the bulge. A simple choice is $\mathbf{u}_0 = 0$ for all design points, provided $\gamma \neq 1$ is used. We have employed this starting point in the first two examples below in order to demonstrate that the algorithm converges to the subsequent design points when starting from the same initial point. However, we have found it to be more efficient (fewer steps needed to converge) if $\mathbf{u}_0$ is chosen on the opposite side of previous bulges. A simple rule for the selection of $\mathbf{u}_0$ for finding the mth design point, thus, is

$$\mathbf{u}_0 = -\varepsilon(\mathbf{u}_1^* + \mathbf{u}_2^* + \cdots + \mathbf{u}_{m-1}^*), \tag{9}$$

where ε is a small positive number in the range 0.2–0.5.

We define by φ_i the angle between $\mathbf{u}_i^*$ and a line from the origin to the foot of the bulge $B_i(\mathbf{u})$, as shown in Fig. 4. The largest value of φ_i occurs when the limit-state surface is spherical. In that case the distance to the foot is also equal to β_i. Using the rule of cosines for the triangle in Fig. 4, we find

$$\varphi_i \leq \cos^{-1}(1 - 0.5\gamma^2). \tag{10}$$

For $\gamma = 1.1$, we have $\varphi_i \leq 66°$. This is the half-angle of an hyper-cone that completely contains the bulge. Any design point found within this cone is potentially spurious.

Another way to determine if a newly found design point is spurious is to compute its distance from previously found design points. If the distance to a previous design point $\mathbf{u}_i^*$ is smaller than or equal to the radius r_i of the corresponding bulge, then the newly found design point is at the foot of the bulge and, therefore, is spurious.

Convergence to a spurious design point usually is an indication that no more genuine design points exist. However, to make sure that this is the case, one may wish to add a new bulge at the spurious design point and continue the search. Naturally, the spurious design point should not be included in the reliability calculations.

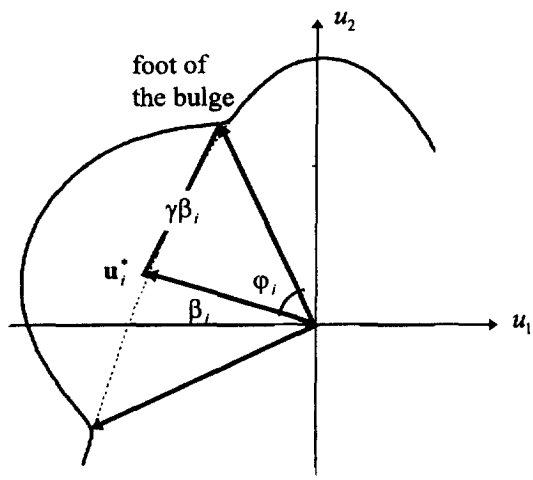

Figure 4. Definition of cone containing the bulge.

4. Example applications

4.1. Example 1: Parabolic limit state

This example is defined by the parabolic limit-state function

$$G(\mathbf{u}) = b - u_2 - \kappa(u_1 - e)^2, \tag{11}$$

where b, κ and e are deterministic parameters and u_1 and u_2 are standard normal variables. By properly selecting b, κ and e, one can define limit-state surfaces that have one or two design points.

Shown in Fig. 1(a) is the limit-state surface $G(\mathbf{u})=0$ for $b=5$, $\kappa=0.5$ and $e=0.1$. The surface has two design points. Using the iHL-RF algorithm with $\mathbf{u}_0=\mathbf{0}$ and a convergence tolerance of 10^{-4} on the reliability index, we obtain, after 10 iterations, the first design point $\mathbf{u}_1^* = [-2.741\ 0.965]^T$ with $\beta_1 = 2.906$ and $\| \nabla G(\mathbf{u}_1^*) \| = 3.011$. The steps are depicted in Fig. 1(a). Now we add the bulge $B_1(\mathbf{u})$ at $\mathbf{u}_1^*$ in accordance to Eqs. (7) and (8) with the parameter values $\gamma=1.1$ and $\delta=0.75$. The new limit-state surface, $G_1(\mathbf{u}) = G(\mathbf{u}) + B_1(\mathbf{u}) = 0$, is shown in Fig. 1(b). Using the iHL-RF algorithm with $G_1(\mathbf{u})$ and employing the same initial point and tolerance, convergence to the second design point is achieved in 7 steps with $\mathbf{u}_1^* = [2.916\ 1.036]^T$, $\beta_2 = 3.094$ and $\| \nabla G(\mathbf{u}_2^*) \| = 2.988$. The steps are shown in Fig. 1(b). Now suppose we proceed further and place a bulge $B_2(\mathbf{u})$ at $\mathbf{u}_2^*$, ignoring the fact that no other genuine design point exists. The corresponding limit-state surface, $G_2(\mathbf{u}) = G(\mathbf{u}) + B_1(\mathbf{u}) + B_2(\mathbf{u}) = 0$, is shown in Fig. 1(c). Starting from $\mathbf{u}_0=0$, the iHL-RF algorithm now converges to $\mathbf{u}_3^* = [-1.6123.721]^T$ with $\beta_3 = 4.055$, as shown in Fig. 1(c). The angles between this and the previous design point vectors are $\cos^{-1}[(\mathbf{u}_1^* \cdot \mathbf{u}_3^*)/(\beta_1\beta_3)] = 47°$ and $\cos^{-1}[(\mathbf{u}_2^* \cdot \mathbf{u}_3^*)/(\beta_2\beta_3)] = 148°$. Obviously $\mathbf{u}_3^*$ is within the cone containing the bulge of the first design point. The distance $\| \mathbf{u}_1^* - \mathbf{u}_3^* \| = 2.978$ between the two design points is less than but close to the radius $r_1 = 1.1 \times 2.906 = 3.197$ of the bulge, thus confirming that $\mathbf{u}_3^*$ is a spurious design point at the foot of bulge $B_1(\mathbf{u})$. At this stage, we are convinced that $\mathbf{u}_1^*$ and $\mathbf{u}_2^*$ are the only legitimate design points for this problem.

In a conventional FORM/SORM application, not knowing the existence of two design points, we would have constructed linear or quadratic approximations at either $\mathbf{u}_1^*$ or $\mathbf{u}_2^*$. The corresponding approximations of the probability of failure $p_f = P[G(\mathbf{u}) \le 0]$ are listed in Table 1. In the present case, having found two design points, FORM and SORM approximations are constructed at *both* these points. The probability of failure is now computed as the probability of the union of the two failure events represented by the two approximating surfaces. The results together with an "exact" solution obtained by Monte Carlo simulation are listed in Table 1.

Table 1
Probability$\times 10^2$ estimates for Example 1

$\mathbf{u}_1^*$ alone		$\mathbf{u}_2^*$ alone		$\mathbf{u}_1^*$ and $\mathbf{u}_2^*$		Monte Carlo
FORM	SORM	FORM	SORM	FORM	SORM	
0.183	0.197	0.099	0.107	0.282	0.304	0.297

Whereas the approximations based on a single design point are in error and dependent on the design point used, the approximations based on the two design points are in close agreement with the Monte Carlo simulation result.

4.2. Example 2: Non-normal random variables

The second example is a well known problem in FORM and SORM. Originally introduced by Hohenbichler and Rackwitz [6], the problem has been discussed by Madsen et al. [1] and Ditlevsen and Madsen [2]. Although the limit-state function is linear in the original space, because of strong non-normality of the random variables, in the standard normal space the limit-state surface is strongly nonlinear and possesses two design points. Conventional FORM and SORM provide results that are inaccurate and strongly dependent on the ordering of the random variables.

The problem is defined by the limit-state function

$$g(x_1, x_2) = 18 - 3x_1 - 2x_2, \tag{12}$$

where x_1 and x_2 are random variables having the joint cumulative distribution function

$$F(x_1, x_2) = 1 - \exp(-x_1) - \exp(-x_2) + \exp[-(x_1 + x_2 + x_1x_2)]\ x_1, x_2 > 0. \tag{13}$$

As described by Hohenbichler and Rackwitz [6], there are (at least) two distinct transformations to the standard normal space:

$$\begin{aligned}(x_1, x_2) \to (u_1, u_2): \quad & u_1 = \Phi^{-1}\{1 - \exp(-x_1)\} \\ & u_2 = \Phi^{-1}\{1 - (1 + x_2)\exp[-(x_2 + x_1x_2)]\}\end{aligned} \tag{14a}$$

and

$$\begin{aligned}(x_1, x_2) \to (u_1, u_2): \quad & u_1 = \Phi^{-1}\{1 - \exp(-x_2)\} \\ & u_2 = \Phi^{-1}\{1 - (1 + x_1)\exp[-(x_1 + x_1x_2)]\}\end{aligned} \tag{14b}$$

where $\Phi^{-1}\{\cdot\}$ denotes the inverse of the standard normal cumulative probability function. These transformations result in the two alternative definitions of the limit-state surface shown in Fig. 5. Although the limit-state function in the original space is linear, in the standard normal space the limit-state surfaces are strongly warped due to the nonlinearity of the transformation. Furthermore, each surface exhibits two distinct design points. Obviously a FORM/SORM analysis using a single design point would lead to erroneous and different solutions for the two alternative transformations. Madsen et al. [1] and Ditlevsen and Madsen [2] discuss this issue and suggest FORM and SORM approximations at the two design points. However, they do not discuss how to obtain the multiple design points for a general problem.

Employing the iHL-RF algorithm with the transformation in Eq. (14a), using $\mathbf{u}_0 = 0$ and a tolerance of 10^{-4}, convergence is achieved in 6 steps to $\mathbf{u}_1^* = [2.782\ 0.0865]^T$ with $\beta_1 = 2.784$. Adding a bulge at $\mathbf{u}_1^*$ and re-applying the iHL-RF algorithm, convergence is achieved in 13 steps

to $\mathbf{u}_2^* = [-1.296\ 3.253]^T$ with $\beta_2 = 3.501$. Employing the transformation in (14b), convergence is achieved in 9 steps to $\mathbf{u}_1^* = [-1.124\ 2.399]^T$ with $\beta_1 = 2.649$, and adding a bulge, convergence is achieved in 9 steps to $\mathbf{u}_2^* = [3.630\ 0.1420]^T$ with $\beta_2 = 3.633$. The FORM and SORM approximations of the estimated probabilities using fittings at single or multiple design points are listed in Table 2. Also listed is the exact solution of the problem obtained by Monte Carlo simulation, as reported by Madsen et al. [1]. It is observed that the estimates based on a single design point strongly depend on the transformation used and the design point found. On the other hand, the SORM estimates based on fittings at the two design points are less dependent on the transformation used and closely agree with the exact solution.

4.3. Example 3: Building with tuned mass damper

It is fortuitous that real structural reliability problems with multiple design points are uncommon. This in fact is the reason for the success of traditional FORM/SORM techniques. Nevertheless, multiple design points do arise in practical applications. Often it is possible to anticipate this situation and we have selected the following problem with that in mind. It is noted, however, that the procedure described in this paper does not require prior knowledge of the existence of multiple design points.

Consider a 10-story building subjected to seismic motion with a tuned mass damper (TMD) placed on its roof, as shown in Fig. 6. The building has floor masses m_i and story stiffnesses k_i,

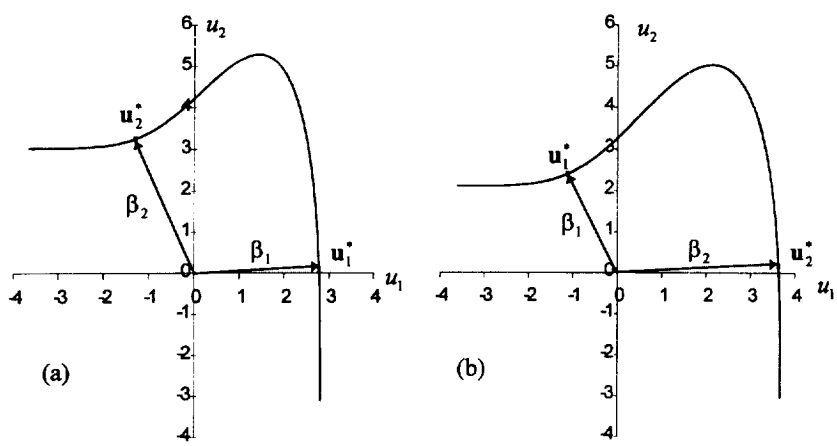

Figure 5. Limit-state surfaces for Example 2: (a) transformation [Eq. (14a)]; (b) transformation [Eq. (14b)].

Table 2
Probability$\times 10^2$ estimates for Example 2

Transformation	$\mathbf{u}_1^*$ alone		$\mathbf{u}_2^*$ alone		$\mathbf{u}_1^*$ and $\mathbf{u}_2^*$		Monte Carlo
	FORM	SORM	FORM	SORM	FORM	SORM	
$(x_1, x_2) \rightarrow (u_1, u_2)$:	0.269	0.279	0.023	0.016	0.292	0.296	0.294
$(x_1, x_2) \rightarrow (u_1, u_2)$:	0.404	0.294	0.014	0.015	0.417	0.308	0.294

$i=1,...,10$, and the TMD has mass m_0 and stiffness k_0. The combined system is assumed to have modal damping ratios ζ_i, $i=0,1,...,10$. The input motion is defined by the pseudo-acceleration response spectrum $A(T,\zeta)=SH(\zeta)a(T)$, where S is a scale factor, $H(\zeta)=0.5+1.5/(40\zeta+1)$ is a damping-dependent amplification factor suggested by Kawashima and Aizawa [7], and $a(T)$ is the normalized pseudo-acceleration response spectrum shape for 5% damping shown in Fig. 7.

The TMD is effective in reducing the dynamic response of the building over a narrow band of frequencies, giving best results when its natural frequency $\omega_0 = \sqrt{k_0/m_0}$ is perfectly tuned to the fundamental frequency of the building, ω_1. As would be the case in a real situation, we assume that the mass, stiffness, and damping properties of both the building and the TMD are uncertain. Due to this uncertainty, perfect tuning between the TMD and the fundamental frequency of the building may not occur. If that happens, the building response would be larger than in the case of

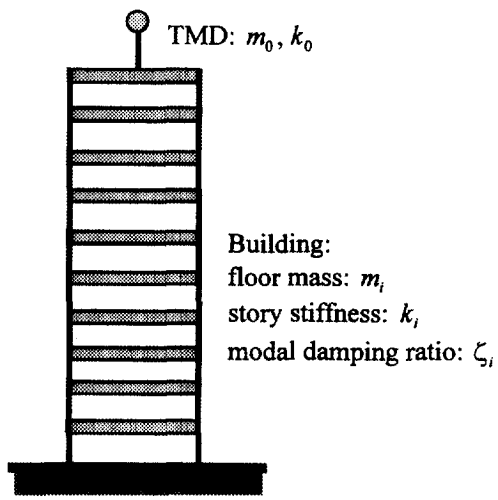

Figure 6. 10-story building with TMD.

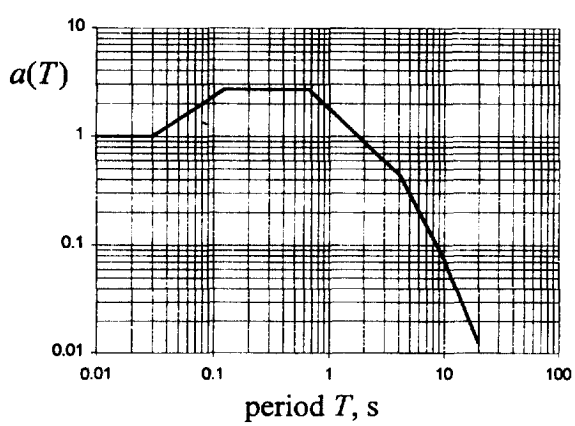

Figure 7. Normalized pseudo-acceleration response spectrum.

perfect tuning. Since the TMD can be "over-tuned" or "under-tuned," one may expect the existence of two design points when considering the reliability of this building.

For reliability analysis, we consider the limit-state function

$$g(\mathbf{x}) = V_0 - V_{\text{base}}(\mathbf{x}), \tag{15}$$

where $\mathbf{x} = (m_0, m_1, \ldots, m_{10}, k_0, k_1, \ldots, k_{10}, \zeta_0, \zeta_1, \ldots, \zeta_{10})$ is the set of 33 random variables of the problem, $V_{\text{base}}(\mathbf{x})$ is the base shear response of the building, which is expressed as an implicit function of $\mathbf{x}$, and V_0 is the allowable threshold. The base shear is computed by combining the modal responses of the 11-degree-of-freedom, combined building–TMD system by the CQC rule (Der Kiureghian [8]). For each set of $\mathbf{x}$ values, this involves eigenvalue analysis of the combined system, computation of the modal contributions to the base shear, and their combination by the CQC rule. For the sake of simplicity of this application, we assume each of the 33 random variables is independent and lognormally distributed with the mean and coefficients of variation (c.o.v.) listed in Table 3. For the mean values listed, the fundamental (first mode) frequency of the structure and the frequency of the TMD are identical and equal to 1.17 Hz, i.e., the mean TMD is perfectly tuned to the first mode of the mean structure. We also assume $S = 0.5$ and $V_0 = 1500$ kips.

Starting from the mean point, an initial run of the iHL-RF algorithm for the above problem converges to the first design point $\mathbf{u}_1^*$, denoted $\mathbf{x}_1^*$ in the original space, in 6 steps with $\beta_1 = 1.06$. Eigenvalue analysis with the property values at $\mathbf{x}_1^*$ reveals the fundamental frequency of the building as 1.15 Hz and the TMD frequency as 1.33 Hz. This corresponds to a case where the TMD is "over-tuned." Next, a bulge is added at $\mathbf{u}_1^*$ and the iHL-RF algorithm is applied again with the initial point selected according to the rule Eq. (9) with $\varepsilon = 0.5$. Convergence is achieved to the second design point $\mathbf{u}_2^*$ ($\mathbf{x}_2^*$ in the original space) in 71 steps with $\beta_2 = 1.71$. Examination of the angle and distance between $\mathbf{u}_1^*$ and $\mathbf{u}_2^*$ reveals that $\mathbf{u}_2^*$ is indeed a legitimate design point. Eigenvalue analysis with the properties at $\mathbf{x}_2^*$ reveals the fundamental frequency of the building as 1.20 Hz and the TMD frequency as 1.03 Hz. This corresponds to a case where the TMD is "under-tuned." Further investigation with a bulge added at $\mathbf{u}_2^*$ reveals no other genuine design point.

Table 4 summarizes the estimates of the probability of failure (i.e., the base shear response exceeding V_0) based on FORM and SORM using either or both design points. These are compared with a Monte Carlo solution listed in the last column, which is based on 2000 simulations. Accounting for both design points is found to significantly improve the failure probability estimate.

Table 3
Mean and coefficient of variation of random variables

Variable	Mean	c.o.v.
$m_1, \ldots, m_{10}$	193 kips/g	0.20
$k_1, \ldots, k_{10}$	1200 kips/in	0.20
m_0	158 kips/g	0.20
k_0	22 kips/in	0.20
$\zeta_0, \zeta_1, \ldots, \zeta_{10}$	0.05	0.30

Table 4
Probability estimates for building with tuned mass damper

$\mathbf{u}_1^*$ alone		$\mathbf{u}_2^*$ alone		$\mathbf{u}_1^*$ and $\mathbf{u}_2^*$		Monte Carlo
FORM	SORM	FORM	SORM	FORM	SORM	
0.145	0.161	0.044	0.058	0.188	0.218	0.213

5. Summary and conclusion

The existence of multiple design points in component reliability analysis could give rise to large errors in FORM and SORM approximations of the failure probability. In this paper, a method is developed to successively find the multiple design points of a reliability problem, when they exist. FORM or SORM approximations at each design point followed by a series system reliability analysis is shown to lead to improved estimates of the failure probability. The method can also be used to ascertain that a design point found is truly the global design point. Example applications show the generality and robustness of the method.

Acknowledgements

This study was performed when the second author was a graduate student at the University of California, Berkeley.

References

[1] Madsen HO, Krenk S, Lind NC. Methods of structural safety. Englewood Cliffs, NJ: Prentice-Hall, 1986.
[2] Ditlevsen O, Madsen HO. Structural reliability methods. New York, NY: J. Wiley & Sons, 1996.
[3] Zhang Y, Der Kiureghian A. Two improved algorithms for reliability analysis. Reliability and optimization of structural systems. In: Rackwitz R, Augusti G, Borri A, editors. Proc. 6th IFIP WG 7.5 working conference on reliability and optimization of structural systems, Assisi, Italy, September 1994. p. 297–304.
[4] Floudas CA, Pardalos PM, editors. State of the art in global optimization: computational methods and applications. Boston, Mass.: Kluwer Academic Pub., 1996.
[5] Luenberger DG. Introduction to linear and nonlinear programming. Reading, Mass: Addison-Wesley, 1986.
[6] Hohenbichler M, Rackwitz R. Nonnormal dependent vectors in structural reliability. J Engineering Mechanics Division, ASCE 1981;107:1127–1238.
[7] Kawashima K, Aizawa K. Modification of earthquake response spectra with respect to damping ratio. In: Proceedings 3rd U.S. National Conference on Earthquake Engineering, Charleston, SC, II 1986. p. 1107–1116.
[8] Der Kiureghian A. A response spectrum method for random vibration analysis of MDF systems. Earthquake Engineering and Structural Dynamics 1981;9(5):419–435.